NOAA Technical Memorandum ERL ETL-266

NOAA LIDAR OBSERVATIONS DURING THE TMDBCE LETHALITY TEST AT WSMR ON 5 FEBRUARY 1993

M.J. Post
L.D. Olivier

Environmental Technology Laboratory
Boulder, Colorado
March 1996

noaa NATIONAL OCEANIC AND ATMOSPHERIC ADMINISTRATION / Environmental Research Laboratories

NOAA Technical Memorandum ERL ETL-266

NOAA LIDAR OBSERVATIONS DURING THE TMDBCE LETHALITY TEST
AT WSMR ON 5 FEBRUARY 1993

Madison J. Post
Lisa D. Olivier

Environmental Technology Laboratory
Boulder, Colorado
March 1996

NOTICE

Mention of a commercial company or product does not constitute an endorsement by NOAA/ERL. Use of information from this publication concerning proprietary products or the tests of such products for publicity or advertising purposes is not authorized.

CONTENTS

NOAA Lidar Observations during the TMDBCE Lethality Test at WSMR on 5 February 1993

Madison J. Post and Lisa D. Olivier

ABSTRACT. The National Oceanic and Atmospheric Administration's (NOAA) pulsed CO_2 Doppler lidar successfully tracked a cloud of liquid triethyl phosphate (TEP) released from an incoming Storm missile. By concentrating on the lowest portion of the cloud, information about the descent of the TEP cloud was obtained. TEP cloud bottom height and a ground track showing the motion of the cloud relative to the lidar were plotted. In addition, lidar measurements were used to guide an instrumented aircraft into the cloud. Improvements for future tests were defined.

1. INTRODUCTION

NOAA's pulsed Doppler lidar participated in the successful Storm demonstration flight and bulk chemical experiment (BCE) on 5 February 1993. The lidar was positioned north of the High Energy Laser Systems test facility (HELSTF) complex at the SE 30 site (32.6604° N latitude, 106.3266° W longitude, and 1217 m elevation), about 12 km northeast of the targeted chemical release point. The mission of the lidar was to track the lower portion of the cloud of liquid triethyl phosphate (TEP) droplets released from the warhead of the incoming Storm missile and to determine whether any of the TEP payload reached the surface in liquid form. The warhead, descending at Mach 5 (about 1 km s^{-1}), was to be "zippered open" by four linear charges beginning at 5 km above ground level (AGL), producing a cloud of TEP about 1 km long.

Instead of mapping out the entire cloud, we chose to concentrate on its lower portion, and to unambiguously define its lower boundary. The plan was to use a scan that swept from left to right over 4° azimuth, step up 0.5° elevation, sweep right to left 4°, step up, etc., eventually filling in a box 4° wide by 2° high before repeating. We actually scanned 11° in azimuth and incremented in elevation by 1°, filling an area 11° wide and 4° high. By moving the entire box with a software "joystick," we could track the cloud and insure that the lowest horizontal sweep did <u>not</u> encounter a portion of the cloud, while at least one of the higher sweeps did. This technique permitted us to bracket the altitude in which the lower cloud boundary could be found.

Another task for the lidar was to help guide an Aeromet aircraft into the liquid cloud, to enable it to measure droplet size spectra with onboard optical probes. In order to accomplish this task, we invested considerable effort in developing new lidar software and in establishing communications with Building 300 (where the range computer and aircraft controller were located). The plan was to send lidar-observed cloud coordinate information over a modem to the range computer every few minutes as input to a predictive program that would enable the aircraft controller to vector the aircraft into the cloud.

An additional task was to provide both range control and the aircraft with up-to-the-minute wind profiles, derived from Doppler lidar plan-position indicator (PPI) scans made just before the test. These data were sent over the same modem, ingested by the range computer, and relayed verbally to the aircraft.

2. LIDAR SENSITIVITY

The lidar threshold of sensitivity was set primarily by the backscatter level of the ambient aerosols. That is, the lidar could detect TEP droplets only if their backscatter coefficient exceeded that of the ambient aerosols (which was about 1×10^{-9} m^{-1} sr^{-1} at cloud bottom). For this test, this statement was held true out to a ground range of about 20 km. Once we were tracking the cloud beyond a ground range of 20 km, we used elevation angles below 5°. At these heights, the absorption of the lidar beam by atmospheric water vapor and CO_2 became an important factor, and the range-squared falloff in received signals began to dominate. In this regime, the backscatter detection threshold rises at a rate proportional to R^2 plus about 1 dB per kilometer. For example, as range increases from 20 to 25 km, minimum detectable backscatter increases by a factor of 5. The mass loading threshold is lower for smaller droplets because they backscatter more efficiently, having more cross-sectional area per unit mass.

3. NARRATIVE

While listening to the BCE countdown over the project network and awaiting the release of TEP from the Storm missile, we positioned the lidar beam at the expected point of cloud bottom, about 4 km AGL at an azimuth of 214.8°. We were recording the video scene with a bore-sighted camera at 6× zoom, filtered with a red filter to increase contrast against the blue sky background. At 1631:19 UTC, we recorded the release of TEP from the warhead, but it occurred slightly to the west of and considerably lower than the expected point. We immediately repositioned the lidar beam to probe cloud bottom and began scanning. The cloud soon began distorting (because of wind shear) and dissipating. After about 3 min, it was difficult to discern against the sky background; after about 4 min 40 s, we lost visual contact completely. The lidar obtained measurements of the bottom of two clouds, *not* simultaneously, until 17 min after the release of TEP, well after the clouds became invisible to the eye.

We continuously tracked the lower portion of a cloud of TEP for ~5 min after release. The cloud was well defined at this point, with returns much greater than the returns from the ambient aerosols. Due to scanner interface miscommunication, we then lost the cloud for ~2 min. From ~7 to 9 min after the event, we again tracked the same cloud bottom, but then from ~9 to 11 min we detected the bottom of a separate cloud that was more to the north of

2

the first cloud and slightly lower in altitude AGL. From 11 to 17 min after the event, we tracked the bottom of the first cloud again, having lost contact with the second one.

Between 12 min and 17 min, the cloud became diffuse, with a few range gates (150-m resolution) of significantly higher intensity imbedded in the more diffuse area of detectable cloud. After 17 min, the cloud signal fell below the detection threshold of the lidar (see previous section). By this time, the lidar-to-cloud ground range had increased from 12 to 22 km.

After losing the cloud signal at the 17-min mark, an attempt was made to search for a distinct cloud, if one was still there, but scanning in a systematic pattern failed to reveal anything but ambient aerosols. We did not lose cloud contact because of loss of signal, since ambient aerosol backscatter was well above system noise, even at a slant range of 25 km (3° elevation angle). At the completion of the measurements, we acquired a final series of backscatter and wind profile data to verify the stability of the atmosphere.

During lidar scanning, when the lidar computer operator observed enhanced backscatter from the cloud, he pressed a key to record the current time and the scanner's azimuth and elevation. He did this in intervals of ~30 s. By doing so for successive clockwise and counterclockwise scanner sweeps and averaging the results, effects of operator response time were reduced. About every 2 min, the averaged azimuth position, lower elevation position, and displayed range to the cloud were then sent by another operator over the modem to Building 300, along with the time of observation.

In general, we were very pleased with the lidar performance, given the high level of uncertainty in cloud longevity and level of backscatter, and the fact that we could not track the cloud visually. The data gaps encountered did not materially affect our ability to characterize important properties of the cloud, namely its longevity and height of cloud bottom. If anything, we erred on the side of caution, sweeping wider in azimuth (~11° sweeps) and stepping higher in elevation (1° increments) than was necessary, thereby sacrificing spatial resolution to insure we would not lose the cloud.

4. RESULTS

Figure 1 shows backscatter profiles taken at 1307 UTC, 3 h and 24 min before the BCE event, and 1717 UTC, 46 min after the event. The second profile (Fig. 1b) was nearly identical to the first (Fig. 1a), except for a layer of subvisual cirrus at 7-8 km above sea level (ASL). Speed and direction for wind profiles acquired at 1555 and 1700 UTC are shown in Table 1. Because differences in the backscatter and wind profiles were so small before and after the event, we assume that they were unchanged throughout the test as well. The dropout in backscatter in Fig. 1 between 5.5 and 6.5 km ASL resulted in missing wind data at these heights because there was not enough signal for the lidar to make accurate wind measurements.
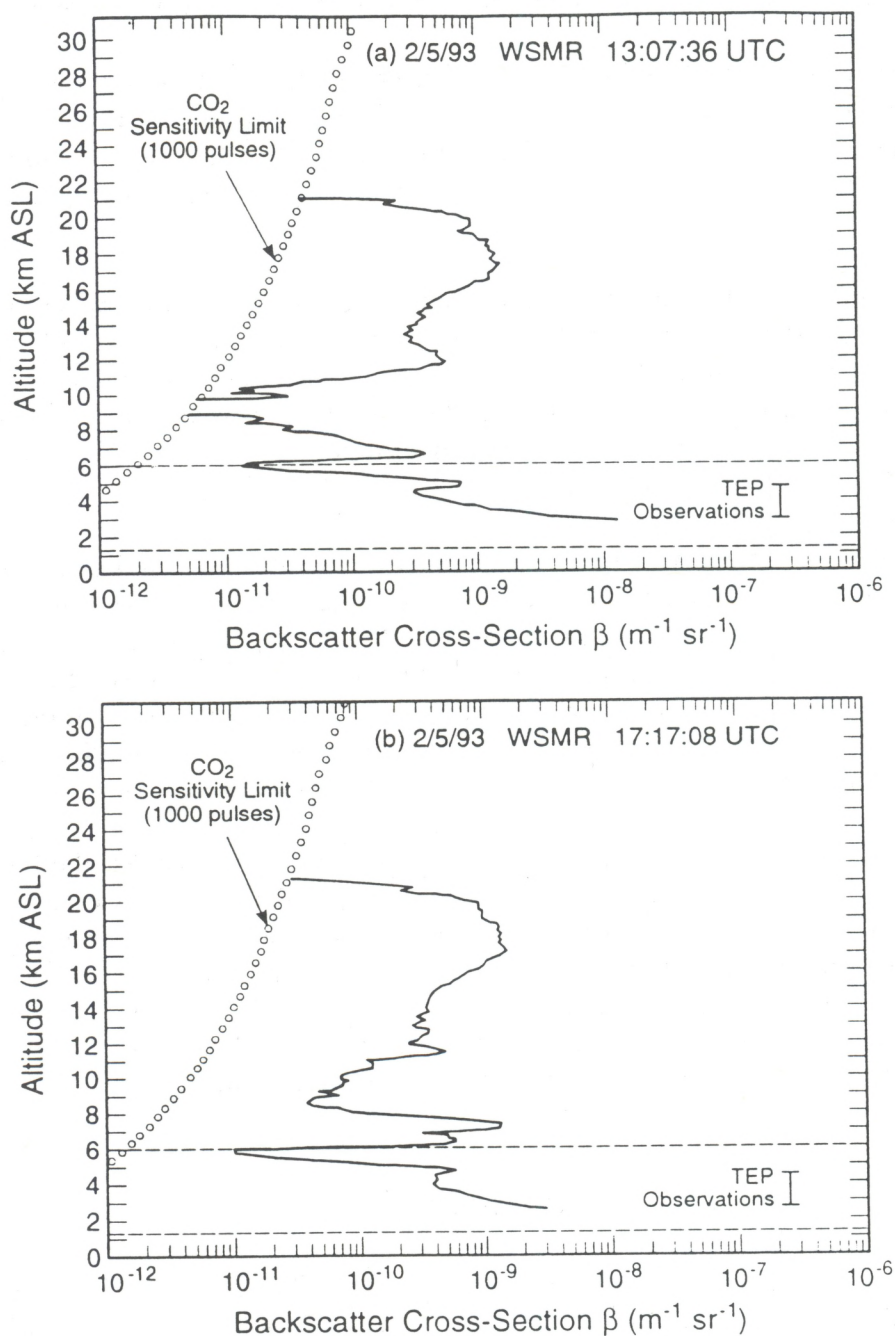
Figure 1.--Lidar backscatter profiles obtained while pointing the lidar beam vertically. Enhanced aerosol layers or cirrus clouds are indicated by higher β values. Lower β values correspond to clean regions of the atmosphere. Ground level is indicated by the lower horizontal dashed line, while the vertical bracket indicates the altitude region over which lidar observations of the lower portion of the TEP cloud were made. The dashed line at 6 km ASL indicates the top of the study region. (a) Backscatter profile taken before the BCE event. (b) Backscatter profile taken after the BCE event.

4

Table 1.--Horizontal winds derived from lidar PPI scans using the Velocity Azimuth Display (VAD) technique.

	Wind Profiles Before and After Storm Demo NOAA Lidar, 5 February 1993, WSMR, New Mexico 45° PPIs			
Altitude (km ASL)	1555 UTC Speed (m s^{-1})	1700 UTC Speed (m s^{-1})	1555 UTC Direction (°)	1700 UTC Direction (°)
2.277	6.6	7.8	25	24
2.489	7.7	8.7	23	27
2.701	9.1	9.4	24	25
2.913	10.7	9.9	21	16
3.125	10.8	9.9	7	3
3.337	10.4	10.3	348	355
3.549	10.7	10.0	331	339
3.761	11.1	11.1	322	326
3.973	12.4	12.1	323	323
4.185	13.9	13.1	319	320
4.397	13.9	13.5	316	317
4.609	14.5	13.9	316	315
4.821	17.2	16.7	318	315
5.033	18.9	17.9	314	314

Using the lidar's angle-calibrated, scanner-mounted video monitor, together with lidar ranging to the initial cloud, we can compute the displacement of the actual TEP cloud with respect to its targeted position. The actual cloud top occurred at 4.09 km AGL instead of 5.00 km AGL, or at 17,414 ft ASL instead of 20,004 ft ASL. It also appeared 0.22 km south and 0.52 km west of the target point. We estimate the cloud to be 0.52 km long 3 s after the event, and 1.344 km long 15 s after the event. With a high-contrast red filter, the cloud became invisible at about 1636:00 UTC, 4 min 41 s after the event.

In Fig. 2, we plot the ground projection of observed cloud "hits." These points are plotted as solid circles, while the x's mark the ground projection of cloud positions sent to Building 300 in near real time to help vector the aircraft. The dashed line in the figure originates at the expected release point, and is a prediction of cloud position obtained from a prediction program that was run before the event. This prediction program uses estimated droplet size and current winds for input. The solid squares correspond to the second cloud that was tracked from 9-11 min after the release of TEP. From the figure, we see that the cloud position data used to help vector the aircraft was accurate, and that the actual cloud advected nearly as predicted. The difference between the predicted trajectory and the actual trajectory was due to the actual release point being different from the planned release point. A complete set of lidar "hits" is given in Table 2, together with the positions of the cloud "hits" in Fig. 2.

Figure 3 shows contoured vertical and horizontal cross sections of the cloud beginning 7 min 10 s after release, averaged over the next 170 s. The cloud is 1.3 km by 0.35 km wide at this point in time.

In addition to the analysis presented above, we created a high resolution 3-dimensional color movie of the intensity-contoured cloud, as observed by the lidar. In this movie, the observer's perspective is from above and to the west of the lidar. The projection of the elevated cloud onto a height-contoured surface map is also shown, complete with major roads and local facilities. Figure 4 is one such movie frame, for 1635:13 UTC, 3 min 54 s after release. The individual frames were used to determine cloud dimensions and average level of backscatter, for estimating mass loading and total mass time histories. We also created another movie by looking at a single frame (like Fig. 4) from 24 different angles, evenly spaced in a circle around frame center. The variable perspective helps one visualize cloud shape much more thoroughly than is possible from a single perspective. We have transcribed the movies from the screen of a scientific workstation to a VHS tape to facilitate dissemination of lidar results. However, there is considerable loss of resolution in the recording process, since the workstation resolution is 800 lines but VHS resolution is only 300 lines.
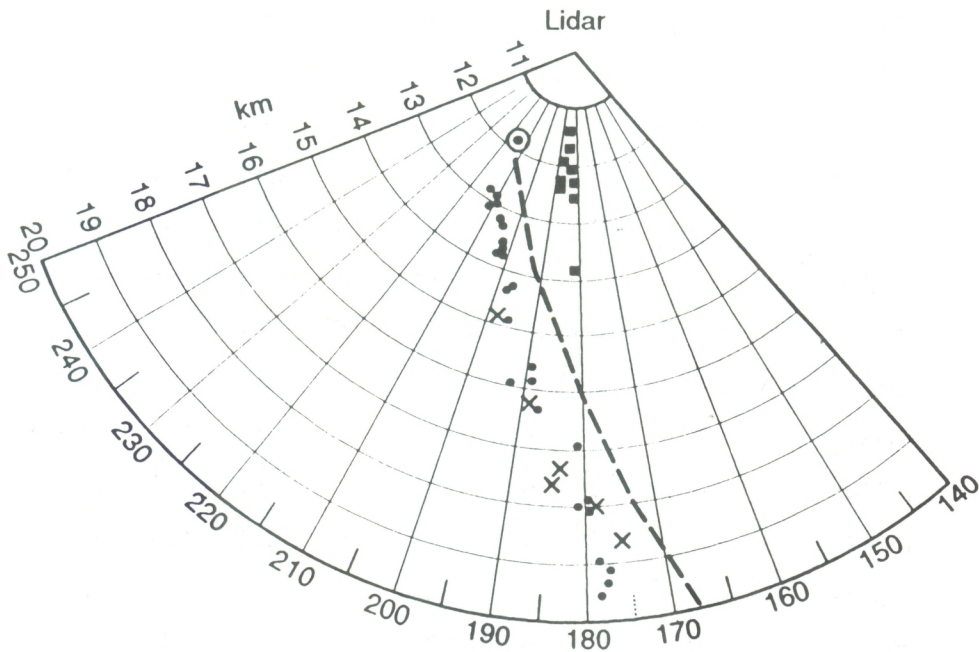
Figure 2.--Ground projection of lidar "hits," points transmitted to the aircraft, the predicted trajectory of the cloud, and the predicted release point are shown. Note that the first range ring is 11 km from the lidar. The square symbols correspond to the second, lower cloud that was tracked by the lidar for ~2 min.

Table 2.--The beginning time (UTC) of the sweep during which a cloud "hit" was obtained, and the time, in seconds, after release. The azimuth (degrees true north), slant range (km), and elevation angle (relative to the lidar) of the center of the "hit." The altitude, latitude, and longitude of the cloud, as derived from the azimuth, elevation angle, and slant range.

	Beginning time of scan	Seconds after release	Azimuth	Slant Range	Elev	Alt AGL	Alt ASL	Lat	Long
First cloud	163214	55	211.00	13.16	14	3.18	4.40	32.562	106.397
	163228	69	210.30	13.38	16	3.69	4.90	32.561	106.396
	163235	76	210.06	13.38	17	3.91	5.13	32.561	106.395
	163243	84	210.48	13.26	13	2.98	4.20	32.560	106.396
	163249	90	214.42	11.37	14	2.75	3.97	32.579	106.393
		90	209.50	13.30	14	3.22	4.43	32.560	106.394
	163256	97	209.45	13.32	15	3.45	4.66	32.560	106.394
	163306	107	209.03	13.24	13	2.98	4.20	32.559	106.393
	163326	127	205.47	14.07	16	3.88	5.09	32.551	106.389
	163354	155	205.63	13.70	15	3.55	4.76	32.553	106.388
	163401	162	202.56	14.08	16	3.88	5.10	32.548	106.382
	163423	184	204.33	13.74	14	3.32	4.54	32.551	106.385
	163429	190	203.54	14.21	15	3.68	4.89	32.547	106.385
	163458	219	201.56	14.09	14	3.41	4.62	32.546	106.380
	163504	225	202.53	14.29	15	3.70	4.92	32.546	106.383
	163523	244	200.47	14.22	14	3.44	4.66	32.544	106.378
	163529	250	196.73	14.85	15	3.84	5.06	32.537	106.371
	163621	302	196.36	14.60	13	3.28	4.50	32.538	106.369
	163627	308	194.90	15.30	14	3.70	4.92	32.532	106.367
	163854	455	189.12	15.90	12	3.31	4.52	32.522	106.353
	163900	461	191.78	16.30	13	3.67	4.88	32.521	106.361
	163946	507	187.74	16.10	11	3.07	4.29	32.520	106.349
	163953	514	187.44	16.60	12	3.45	4.67	32.516	106.349
		514	183.96	18.10	12	3.76	4.98	32.502	106.340
	163959	520	180.93	17.40	13	3.91	5.13	32.508	106.330

Table 2.--(Con't)

	Beginning time of scan	Seconds after release	Azimuth	Slant Range	Elev	Alt AGL	Alt ASL	Lat	Long
Second, lower cloud	164021	542	186.44	11.50	11	2.19	3.41	32.560	106.340
	164028	549	186.10	12.70	12	2.64	3.86	32.549	106.341
	164034	555	180.83	12.60	13	2.83	4.05	32.550	106.328
	164054	575	185.05	11.90	11	2.27	3.49	32.556	106.338
	164101	582	186.03	12.20	12	2.54	3.75	32.554	106.340
	164113	594	186.13	12.60	12	2.62	3.84	32.550	106.341
	164135	616	182.60	12.20	10	2.12	3.34	32.553	106.332
	164141	622	182.60	12.70	11	2.42	3.64	32.549	106.333
	164214	655	182.52	14.06	11	2.68	3.90	32.537	106.333
First cloud	164300	701	180.00	18.00	10	3.13	4.34	32.501	106.327
	164305	706	180.60	18.00	10	3.13	4.34	32.501	106.329
	164340	741	179.50	18.10	10	3.14	4.36	32.500	106.325
	164417	778	177.32	19.30	10	3.35	4.57	32.490	106.317
	164507	828	177.70	18.30	9	2.86	4.08	32.498	106.319
	164509	830	177.30	19.90	10	3.46	4.67	32.485	106.317
	164537	858	175.80	19.60	9	3.07	4.28	32.487	106.312
	164608	889	176.15	19.40	9	3.03	4.25	32.489	106.313
	164610	891	168.10	22.30	10	3.87	5.09	32.467	106.278
	164642	923	168.70	21.50	7	2.62	3.84	32.472	106.282
	164648	929	174.90	19.60	8	2.73	3.94	32.487	106.308
	164702	943	174.30	19.60	10	3.40	4.62	32.488	106.306
	164710	951	170.50	21.00	6	2.20	3.41	32.475	106.290
		951	173.90	23.00	6	2.40	3.62	32.456	106.301
	164724	965	172.20	22.40	7	2.73	3.95	32.463	106.294
	164731	972	171.70	21.60	9	3.38	4.60	32.471	106.294
		972	167.00	21.40	9	3.35	4.56	32.475	106.276
	164746	987	170.00	22.50	6	2.35	3.57	32.462	106.285

Table 2--(Cont'd)

	Beginning time of scan	Seconds after release	Azimuth	Slant Range	Elev	Alt AGL	Alt ASL	Lat	Long
First cloud	164753	994	174.20	19.70	7	2.40	3.62	32.486	106.306
		994	170.00	21.40	7	2.61	3.83	32.473	106.287
	164759	1000	172.90	20.50	8	2.85	4.07	32.479	106.300
		1000	174.10	21.70	8	3.02	4.24	32.468	106.303
	164806	1007	172.70	22.00	9	3.48	4.70	32.467	106.297
	164828	1029	169.10	22.70	7	2.77	3.98	32.462	106.281
Cloud is very diffuse	164835	1036	169.13	20.90	8	2.91	4.13	32.478	106.285
	164842	1043	168.38	20.90	9	3.27	4.49	32.479	106.282
	164857	1058	172.65	23.00	6	2.40	3.62	32.457	106.295
		1058	169.80	23.00	6	2.40	3.62	32.458	106.283
	164907	1068	172.60	20.50	7	2.50	3.72	32.479	106.299
	164946	1107	172.50	27.10	6	2.83	4.05	32.420	106.289
	164953	1114	171.20	26.70	7	3.25	4.47	32.423	106.283
	165000	1121	169.80	26.50	8	3.69	4.91	32.428	106.277
	165007	1128	173.80	23.10	9	3.61	4.83	32.457	106.300
	165022	1143	170.11	27.90	6	2.92	4.13	32.415	106.276
	165029	1150	172.30	28.20	7	3.44	4.65	32.411	106.287
	165035	1156	170.40	22.30	8	3.10	4.32	32.465	106.287
	165057	1178	170.00	26.90	6	2.81	4.03	32.424	106.277
	165104	1185	170.00	27.80	7	3.39	4.60	32.416	106.276
	165129	1210	163.40	28.90	6	3.02	4.24	32.413	106.239
	165136	1217	167.70	28.00	7	3.41	4.63	32.416	106.264
	165149	1230	163.80	26.80	9	4.19	5.41	32.432	106.248
	165211	1252	162.20	26.60	7	3.24	4.46	32.435	106.241
	165218	1259	162.90	27.70	8	3.86	5.07	32.425	106.241
	165240	1281	164.60	28.00	6	2.93	4.14	32.419	106.248

Table 2--(Cont'd)

	Beginning time of scan	Seconds after release	Azimuth	Slant Range	Elev	Alt AGL	Alt ASL	Lat	Long
Cloud is very diffuse	165247	1288	162.20	28.20	7	3.44	4.65	32.421	106.236
	165253	1294	164.90	27.80	8	3.87	5.09	32.422	106.250
	165300	1301	166.31	25.40	9	3.97	5.19	32.441	106.263
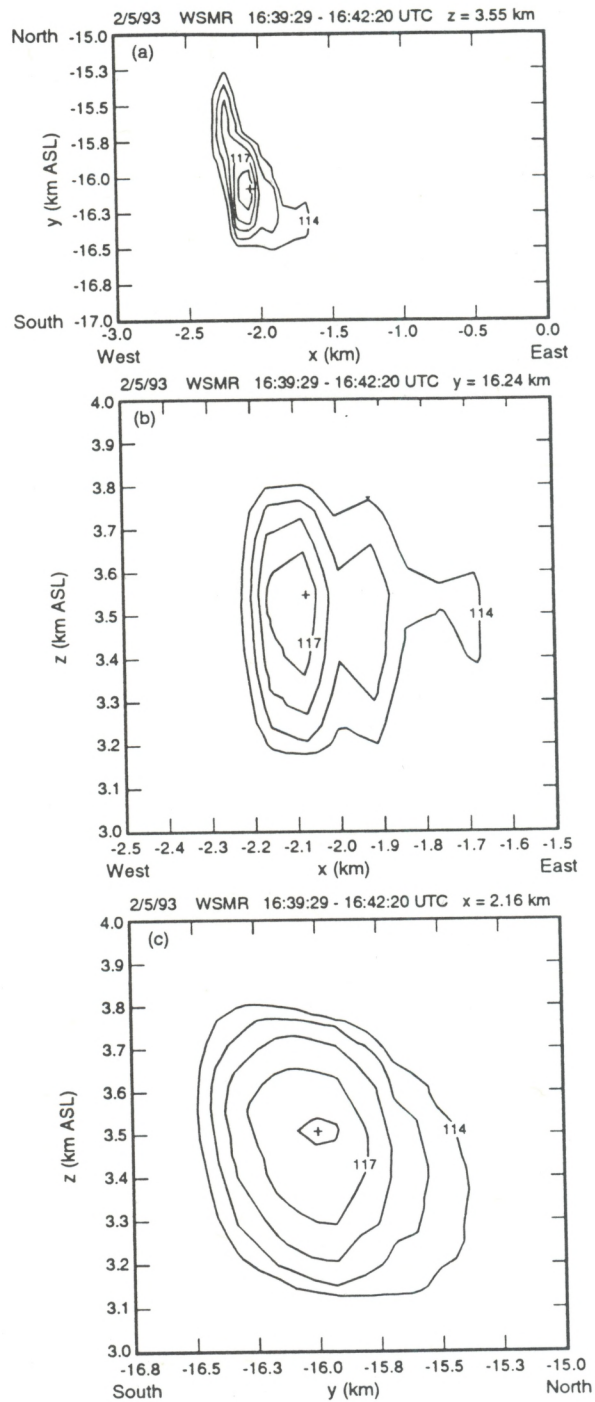
Figure 3.--Cross sections of the TEP cloud. Contours are lidar backscattered signal intensity values (dB), which have been converted to mass loading estimates. All distances are relative to the lidar. (a) Horizontal slice through the cloud at 3.55 km AGL. (b) East-west oriented vertical slice through the cloud, 16.24 km south of the lidar. (c) North-south oriented vertical slice through the cloud, 2.16 km west of the lidar.
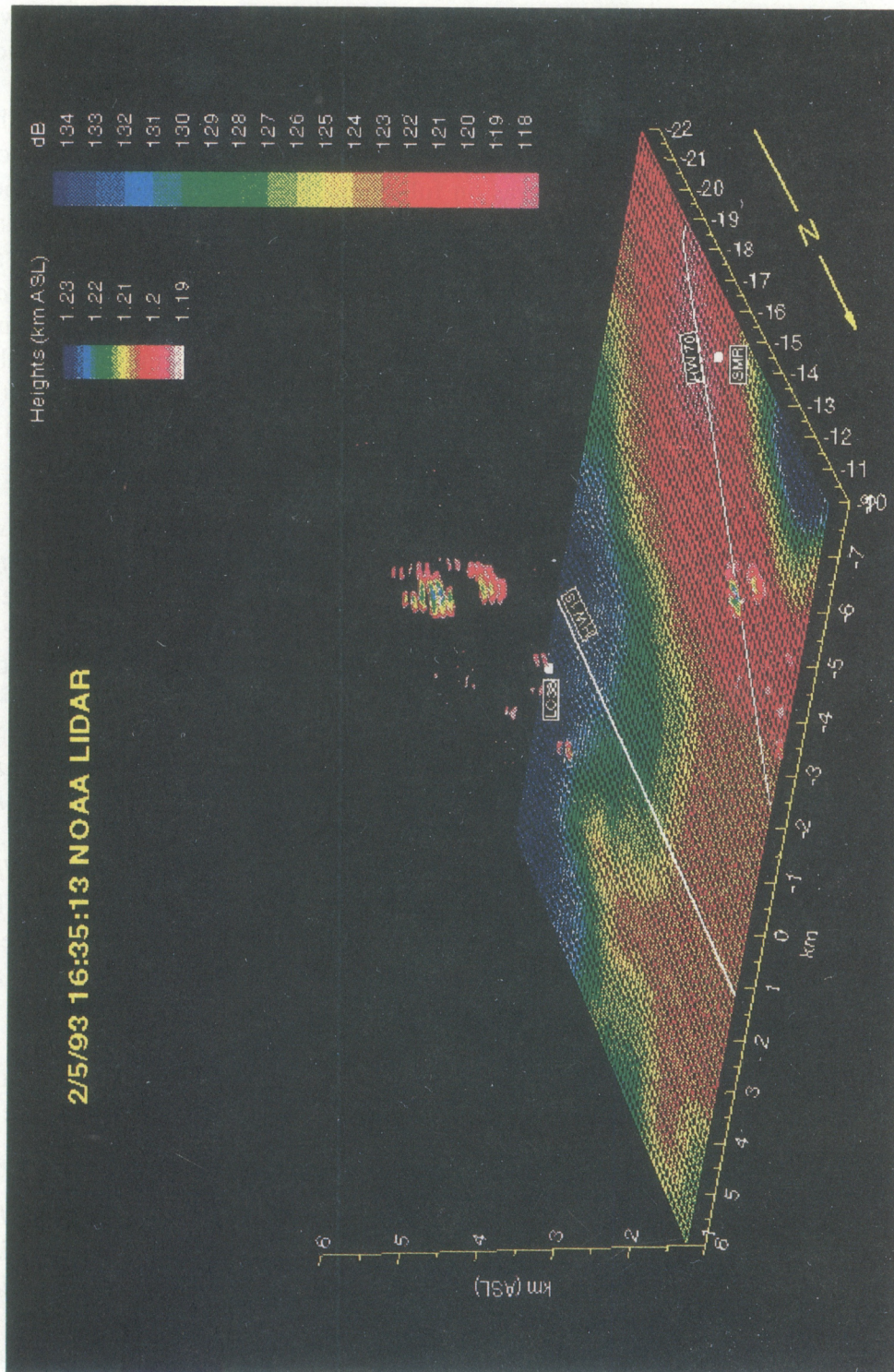
Figure 4.--Three-dimensional visualization of the cloud bottom as measured by the lidar at 1635:13 UTC, ~4 min after the release of TEP. The lidar is located at x = 0, y = 0, and z = 0. The viewer's perspective is from the northwest. The mesh surface at the bottom of the grid is the terrain in kilometers ASL, with major landmarks superimposed. The shape of the cloud is projected downward onto the terrain. At this time, the cloud is over Highway 70. The contours of the cloud and cloud projection are backscatter values in decibels. Higher decibel values (>125) occur in the upper part of cloud bottom and gradually decrease with time.

5. IMPROVEMENTS FOR FOLLOWING TESTS

Several operational procedures should be improved or changed for future tests, based on what we learned at this test. These are explained below, with some comments on whether these ideas were tried during future tests and if they did in fact improve our performance.

Because we parked the lidar beam at the azimuth and elevation coordinates of the expected cloud bottom, because the TEP release occurred at a lower altitude than expected, and because the bore-sighted video camera was on full zoom, we did not observe the bottom of the cloud until about 15 s after T_0. As a result, we lost some time in choosing the initial lidar scan pattern. *In future tests, the camera should be configured at an intermediate zoom setting and its video monitor should be overlaid with a grid of preprogrammed scans to allow the operators to move more quickly to the most appropriate scan.* Our experience at future tests has shown that positioning the camera at an intermediate zoom did improve our ability to find the initial cloud bottom. It is important, however, to know the zoom factor so that estimations of the cloud size can be made from video images. We have not yet used a grid of preprogrammed scans overlaid on the video monitor.

A remote monitor from one of the Aerospace, Inc., cameras should be set up inside the lidar trailer to assist the lidar crew in acquiring the cloud if they lose it. Some indication of camera pointing is needed, such as azimuth and elevation (true or magnetic). In subsequent tests, we were unable to acquire the remote monitor from Aerospace, Inc., but we have found that the prediction program that we run on a personal computer in the trailer has helped us to find the cloud if momentarily lost.

On the lidar's real-time display, the intensity threshold should be slightly raised to better distinguish TEP returns from those of ambient aerosols. More attention should be paid to using the tab keys frequently to identify cloud position. Cloud position information should be sent directly to the aircraft, eliminating range control as an intermediate data handler. Setting the threshold to distinguish the TEP returns and using the tab key to note the cloud position are routine now. We can give information about cloud position directly to the pilot of the aircraft, but White Sands Missile Range (WSMR) staff must actually vector the aircraft to the cloud, so we cannot eliminate range control as an intermediate data handler.

The line printer used in the 5 February 1993 case was replaced with one that does not jam so easily. Jamming caused significant delays in relaying cloud position during the 5 February 1993 test.

The scan pattern within the azimuth and elevation block containing the cloud should alternate between horizontal and vertical volumes, each with about a 15-s period. This will permit tracking cloud bottom __and__ gaining more insight on cloud structure and dimensions. We have since alternated between horizontal and vertical volumes during some of the subsequent tests. This scheme did allow us to provide more information about the structure of the cloud. *The breadth of the scan patterns should be reduced to increase the percentage*

14

of time the lidar is acquiring cloud data. In subsequent tests, this change did allow us to acquire more volumes of data. *Finally, when the cloud bottom is lost or dissipates, a search should be made at higher elevation angles for remnants of the main body of the cloud.* In subsequent tests, the cloud remained visible much longer than during this test, so an additional search was not needed.

6. CONCLUSIONS

The ground tracks for two separate clouds were successfully determined. Cross sections showing the general shape of the cloud were plotted. Estimates of mass TEP loading (peak and average) were calculated for the cloud bottom region (not shown in this version of the report). The bracketed height interval in which the cloud bottom occurred was determined by the scanning strategy of scanning into the cloud and then scanning below the cloud. We believe the lidar did a credible job in tracking the larger droplets of TEP in the lower portion of the cloud, although those droplets were not detected visually or by other sensors.

7. ACKNOWLEDGMENTS